Simulation Prediction of Heat Transport with Machine Learning in Tokamak Plasmas

Hui Li(李慧)[1*], Yan-Lin Fu(付艳林)[2], Ji-Quan Li(李继全)[3], and Zheng-Xiong Wang(王正汹)[1*]

[1]*Key Laboratory of Materials Modification by Laser, Ion, and Electron Beams (Ministry of Education), School of Physics, Dalian University of Technology, Dalian 116024, China*
[2]*State Key Laboratory of Molecular Reaction Dynamics and Center for Theoretical and Computational Chemistry, Dalian Institute of Chemical Physics, Chinese Academy of Sciences, Dalian 116023, China*
[3]*Southwestern Institute of Physics, Chengdu 610041, China*

(Received 6 July 2023; accepted manuscript online 21 November 2023)

Machine learning opens up new possibilities for research of plasma confinement. Specifically, models constructed using machine learning algorithms may effectively simplify the simulation process. Previous first-principles simulations could provide physics-based transport information, but not fast enough for real-time applications or plasma control. To address this issue, this study proposes SExFC, a surrogate model of the Gyro-Landau Extended Fluid Code (ExFC). As an extended version of our previous model ExFC-NN, SExFC can capture more features of transport driven by the ion temperature gradient mode and trapped electron mode, using an extended database initially generated with ExFC simulations. In addition to predicting the dominant instability, radially averaged fluxes and radial profiles of fluxes, the well-trained SExFC may also be suitable for physics-based rapid predictions that can be considered in real-time plasma control systems in the future.

DOI: 10.1088/0256-307X/40/12/125201

Artificial intelligence is currently regarded as a Priority Research Opportunity (PRO) in fusion control,[1,2] which has been effectively implemented in plasma-shape parameter reconstruction, surrogate model construction, and perturbation detection.[3–5] As high-performance computing resources become more powerful, machine learning approaches are regarded as essential tools for modeling and big data exploitation, including analysis and operation of fusion plasmas.[6–9] The emergence of these methods provides opportunities and applications for the exploration of complex phenomena. For instance, in micro-turbulence simulation models, the application of neural networks (NNs) for the construction of fast surrogate models has been proposed[10,11] in recent work.

Much effort has recently been devoted to explaining the underlying physics of turbulent transport in tokamak plasmas. Direct numerical simulations, which have also become powerful tools in turbulence research, have revealed a great deal about it. Within the discharge time scales, time-evolved tokamak simulations have also been performed typically using 'integrated modelling'.[12] An essential part of integrated models is the prediction of turbulent fluxes, especially in the tokamak core, where plasma micro-instabilities usually dominate the transport[13,14] process. For normal calculation of tokamak discharges, nevertheless, it requires huge computational cost to compute fluxes, especially using nonlinear models. Benefiting from the development of machine learning, these approaches have been applied in plasma research in various fields, such as the regression of energy confinement scaling nonlinearly,[15] database construction,[16] rapid determination of equilibria parameters,[17] reconstruction of temperature profile,[18] analysis of charge exchange spectrum on the JET device,[19] classification of disruption,[20] and development of surrogate models.[21,22]

Motivated by the need for further prediction of transport characteristics caused by micro-turbulence with real-time character, in this work, the properties of electron heat transport, mainly in L-mode plasma conditions, are firstly introduced, using the Extended Fluid Code (ExFC). In particular, the electron heat pinch is found, which can be compared with theoretical and simulation research.[23] In order to shorten the execution cost of ExFC, ExFC-NN[24] is extended. Here, a surrogate model based on machine learning has been raised, which is named as SExFC. The time cost of building a machine learning-based surrogate model mainly lies in the training process, while the evaluation process is pretty rapid, which in our case only costs around several microseconds. SExFC can predict the type of dominant turbulence [including pure ion temperature gradient (ITG), pure trapped electron mode (TEM), as well as mixed ITG and TEM], radially averaged fluxes [$\langle Q_e \rangle_r$, $\langle Q_i \rangle_r$ and $\langle \Gamma \rangle_r$], and radial profiles of perturbations [$\tilde{T}_i(r)$, $\tilde{T}_e(r)$, and $\tilde{n}(r)$], corresponding radial profiles of fluxes [$Q_i(r)$, $Q_e(r)$, and $\Gamma(r)$], and so on.

ExFC is a recently developed global-type transport gyro-Landau fluid code containing the 3-dimensional finite difference approach. ExFC aims to investigate the physics of flux (external source terms)/gradient-driven turbulence in tokamak plasmas with multi-scale and multi-mode prop-

*Corresponding authors. Email: huilee@dlut.edu.cn; zxwang@dlut.edu.cn
© 2023 Chinese Physical Society and IOP Publishing Ltd

erties. The functions are simulated as follows:[25–28]

$$d_t n_\mathrm{e} = -\omega_{dte}(n_0\varphi - T_{\mathrm{e}0}n_\mathrm{e} - n_0 T_\mathrm{e}) + D_n\nabla_\perp^2 n_\mathrm{e}, \quad (1)$$

$$d_t T_\mathrm{e} = -T_{\mathrm{e}0}\omega_{dte}[(\varsigma-1)(\varphi - \tau_{en}n_\mathrm{e}) - (2\varsigma-1)T_\mathrm{e}] - (\varsigma-1)\sqrt{8m_\mathrm{e}T_{\mathrm{e}0}/m_\mathrm{i}\pi}|\nabla_\parallel|T_\mathrm{e} + D_\mathrm{Te}\nabla_\perp^2 T_\mathrm{e}, \quad (2)$$

$$d_t\Omega = -T_{\mathrm{i}0}a(\partial_r \ln n_0 + \partial_r \ln T_{\mathrm{i}0})\partial_\theta\nabla_\perp^2\varphi + f_\mathrm{c}a\partial_r \ln n_0\partial_\theta\varphi - \nabla_\parallel v_\parallel + \omega_{di}[(1+f_\mathrm{c}/\tau)\varphi + T_\mathrm{i} + f_t\tau_{in}n_\mathrm{e}] + f_t\omega_{dte}(\varphi - T_\mathrm{e} - \tau_{en}n_\mathrm{e}) + D_U\nabla_\perp^2\Omega, \quad (3)$$

$$d_t v_\parallel = -\nabla_\parallel T_\mathrm{i} - f_t\tau_{in}\nabla_\parallel n_\mathrm{e} - (1+f_\mathrm{c}/\tau)\nabla_\parallel\varphi + D_v\nabla_\perp^2 v_\parallel, \quad (4)$$

$$d_t T_\mathrm{i} = -T_{\mathrm{i}0}(\varsigma-1)\nabla_\parallel v_\parallel + T_{\mathrm{i}0}\omega_{di}\{(\varsigma-1)[(1+f_\mathrm{c}/\tau)\varphi + f_t\tau_{in}n_\mathrm{e}] + (2\varsigma-1)T_\mathrm{i}\} - (\varsigma-1)\sqrt{8T_{\mathrm{i}0}/\pi}|\nabla_\parallel|T_\mathrm{i} + D_\mathrm{Ti}\nabla_\perp^2 T_\mathrm{i}, \quad (5)$$

in which n_e is the normalized electron density, T_e is the electron temperature, Ω is the vorticity defined as $\Omega = [f_\mathrm{c}n_0(\varphi - \langle\varphi\rangle)]/T_{\mathrm{e}0} - \nabla_\perp^2\varphi$, $v_\parallel$ is the parallel ion velocity and T_i is the ion temperature. Furthermore, electrostatic potential averaged around the magnetic surface is represented by the symbol $\langle\varphi\rangle$. It is mentioned that vorticity contains both electron and ion temperature which means TEM and toroidal ITG modes are coupled. As a result, both ITG and TEM may be included in the multimode system. The gyroBohm type is applied as the normalization. The time coordinate is normalized by $a/c_{\mathrm{s}0}$ ($c_{\mathrm{s}0} = (T_{\mathrm{i}0}/m_\mathrm{i})^{1/2}$, ion sound speed):

$$\left(t\frac{c_{\mathrm{s}0}}{a},\ \frac{r}{\rho_{\mathrm{s}0}},\ \rho_{\mathrm{s}0}\nabla_\perp,\ a\nabla_\parallel\right) \to (t,\ r,\ \nabla_\perp,\ \nabla_\parallel), \quad (6)$$

and the spatial coordinate is normalized by $\rho_{\mathrm{s}0}$ ($\rho_{\mathrm{s}0} = m_\mathrm{i}c_{\mathrm{s}0}/e_\mathrm{i}B_0$, ion sound gyroradius):

$$\frac{a}{\rho_{\mathrm{s}0}}\left(\frac{n_\mathrm{e}}{n_0},\ \frac{T_\mathrm{e}}{T_{\mathrm{e}0}},\ \frac{e\varphi}{T_{\mathrm{e}0}},\ \frac{v_\parallel}{c_{\mathrm{s}0}},\ \frac{T_\mathrm{i}}{T_{\mathrm{i}0}}\right) \to (n_\mathrm{e},\ T_\mathrm{e},\ \varphi,\ v_\parallel,\ T_\mathrm{i}). \quad (7)$$

The q profile is displayed as an example in Fig. 1.

The radial profiles are formed:

$$n_0(r) = n_\mathrm{c}\exp\{-(\Delta_r/L_n)\tanh[(r-r_0)/\Delta_r]\}, \quad (8)$$

$$T_{\mathrm{s}0}(r) = T_{\mathrm{sc}}\exp\{-(\Delta_{rs}/L_{\mathrm{Ts}})\tanh[(r-r_0)/\Delta_{rs}]\}. \quad (9)$$

Here, the subscript label s stands for the species of electrons and ions, the label c corresponds to the plasma center at the magnetic axis. The ratios of temperature and density are displayed as

$$\tau = T_{\mathrm{e}0}/T_{\mathrm{i}0}, \quad \tau_{en} = T_{\mathrm{e}0}/n_0, \quad \tau_{in} = T_{\mathrm{i}0}/n_0. \quad (10)$$

The subscript 0 represents the equilibrium quantity; a is the minor radius, and R is the major radius. The inverse aspect ratio is represented as $\varepsilon = a/R$. Operator $f_t = 2\sqrt{2r/R}/\pi$ is the fraction of trapped electrons, then the fraction of passing electrons is $f_\mathrm{c} = 1 - f_t$. Operators of trapped electron precession drift and ion magnetic drift are defined as $\omega_{dte} = 2\varepsilon\lambda_t q r^{-1}\partial_\phi$ and $\omega_{di} = 2\varepsilon(\cos\theta r^{-1}\partial_\theta + \sin\theta\partial_r)$, respectively. The precession frequency of trapped electrons is $\lambda_t = 1/4 + 2\,s/3$, in which the magnetic shear is defined as $s = rdq/qdr$. The other operators are expressed as follows:

$$d_t f = \partial_t f + [\varphi, f], \quad (11)$$

$$[\varphi, f] = r^{-1}(\partial_r\varphi\partial_\theta f - \partial_\theta\varphi\partial_r f), \quad (12)$$

in which f represents any field variable. The adiabatic compression index is $\varsigma = 5/3$. The diffusivity terms, $D_n = D_\mathrm{Te} = D_U = D_v = D_\mathrm{Ti} = 4.8\times10^{-3}$, are included to damp smaller-scale fluctuations. Equations (1)–(5) are numerically solved with ExFC in toroidal coordinate (r, θ, ϕ) and the simulation domains are $[L_r, L_\theta, L_\phi] \approx [a, 2\pi, 2\pi]$. More details about the code and models are included in our previous work.[24] In the following, all the results are calculated with usages of the gradient-driven version ExFC.

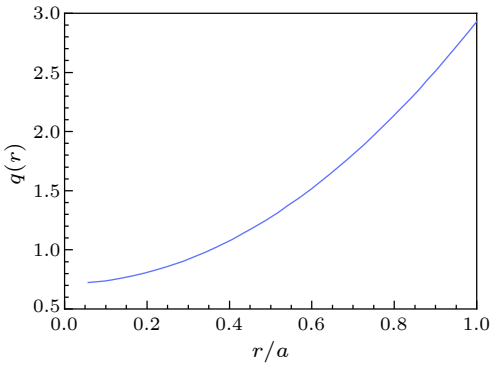

Fig. 1. Schematic of the q profile.

In our previous research, a credible NN-based model, ExFC-NN, has been developed.[29] A clear and detailed methodology of the ExFC-NN construction is described in our previous work (Ref. [29]). The electrostatic ITG and TEM turbulence system is taken into account in ExFC-NN. The well-trained ExFC-NN perfectly reproduces and predicts what the ExFC can do while taking less calculation time. Detailed in Table 1, the applications of previous ExFC-NN have been concluded with predictions of the type of dominant turbulence (including pure ITG, pure TEM as well as the mixed ITG and TEM), radially averaged fluxes ($\langle Q_\mathrm{e}\rangle_r$, $\langle Q_\mathrm{i}\rangle_r$, and $\langle\Gamma\rangle_r$), and radial profiles of perturbations [$\tilde{T}_\mathrm{i}(r)$, $\tilde{T}_\mathrm{e}(r)$, and $\tilde{n}(r)$] as well as corresponding radial profiles of fluxes ($Q_\mathrm{i}(r)$, $Q_\mathrm{e}(r)$, and $\Gamma(r)$). The average region is in [0.3, 0.8] and time is also averaged in the nonlinear steady stage. Furthermore, the ExFC-NN has been considered to realize experimental analysis of the HL-2A fusion device which may provide reference for the design of experimental parameters. In this work, more plasma parameters are contained, i.e., the database has been expanded. Additional plasma physics is taken into account as a result. The extended ExFC-NN is named as SExFC with the differences between ExFC-NN and SExFC detailed in Table 1. Most importantly, it is critical to select the appropriate plasma parameters for constructing the dataset. Figure 2 shows the process of constructing the database and model in detail. According to the flow chart, further points are added iteratively. Though in the nonlinear steady state, the simulation results still have slight fluctuations in the nonlinear evolution.

Table 1. Comparisons between ExFC-NN and SExFC.

	ExFC-NN	SExFC
Input parameters	$R/L_n, R/L_{\rm Te}, R/L_{\rm Ti}$, $T_{\rm i0}(r), T_{\rm e0}(r), n_0(r), \varepsilon$	$R/L_n, R/L_{\rm Te}, R/L_{\rm Ti}$, $T_{\rm i0}(r), T_{\rm e0}(r), n_0(r), q(r), s, \varepsilon$
Output 1	Dominant type of turbulence (ITG, TEM, ITG & TEM)	Dominant type of turbulence (ITG, TEM, ITG & TEM)
Output 2	Radial averaged fluxes $\langle Q_{\rm e}\rangle_r, \langle Q_{\rm i}\rangle_r, \langle \Gamma\rangle_r$	Radial averaged fluxes $\langle Q_{\rm e}\rangle_r, \langle Q_{\rm i}\rangle_r, \langle \Gamma\rangle_r$
Output 3	Radial profiles of perturbations and fluxes $\tilde{T}_{\rm i}(r), \tilde{T}_{\rm e}(r), \tilde{n}(r), Q_{\rm i}(r), Q_{\rm e}(r), \Gamma(r)$	Radial profiles of perturbations and fluxes $\tilde{T}_{\rm i}(r), \tilde{T}_{\rm e}(r), \tilde{n}(r), Q_{\rm i}(r), Q_{\rm e}(r), \Gamma(r)$
Output 4	Experimental process	Experimental process
Output 5		Real-time evolution of fluxes and perturbations

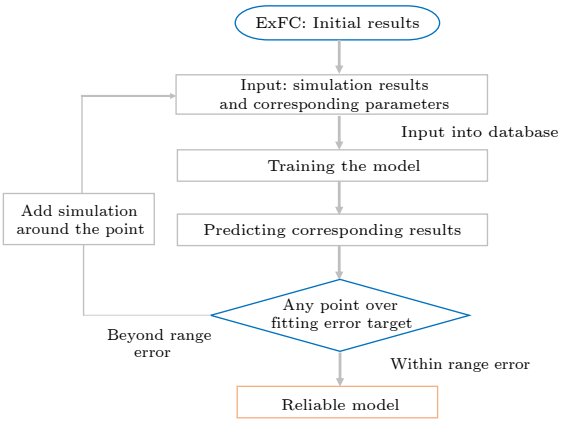

Fig. 2. Schematic diagram for the construction of simulation results in order to obtain a reliable model.

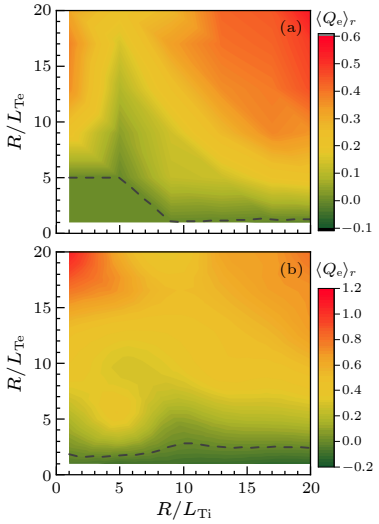

Fig. 3. Contour plots of electron heat transport $\langle Q_{\rm e}\rangle_r$ in the plane of $(R/L_{\rm Ti}, R/L_{\rm Te})$ with (a) $R/L_n = 1$ and (b) $R/L_n = 9$.

As for the description in the introduction, enhancing the understanding of physical mechanisms of anomalous transport, through both ion and electron channels, is of central importance for achievement of burning plasmas. The transport of heat across flux surfaces in magnetic fusion experiments has been observed in previous research. Accordingly, a thorough comprehension of the mechanisms of turbulent transport and improvement of energy confinement is of great significance from both theoretical and experimental points of view. An anomalous pinch (a net inward flow of particle/energy transport channel) was observed in various devices, such as ASDEX-Upgrade,[30] Tore Supra,[31] DIII-D,[32] and JET,[33] and attracted particular attention. Particle transport has been researched in our previous work, therefore, in the present research, the phenomenon of electron heat transport is described with simulations. The contour plots of radial averaged electron heat transport $\langle Q_{\rm e}\rangle_r$ for given $R/L_n = 1$ and $R/L_n = 9$ are separately illustrated in Fig. 3. Directly, the density gradient R/L_n may cause more electron heat transport both in an outward and inward direction. In some parameter regions, $\langle Q_{\rm e}\rangle_r \sim 0$ is observed. As shown in Ref. [23], the inward heat flows in tokamaks were analyzed. For local quasilinear heat fluxes, the expression was separated as follows:[23,34]

$$\boldsymbol{q}_j = -n_j\chi_{jj}\nabla T_j + T_j\chi_{jn}\nabla n_j - \boldsymbol{V}_j n_j T_j, \qquad (13)$$

in which j denotes species.

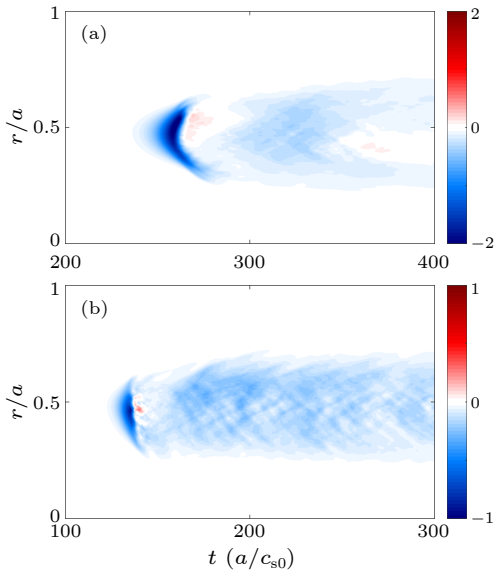

Fig. 4. Time evolution of radial electron heat flux $Q_{\rm e}$ with $R/L_n = 9$: (a) $R/L_{\rm Ti} = 1$, (b) $R/L_{\rm Ti} = 9$.

However, it is not unique because of the coefficients which depend on the profile scale lengths nonlinearly.

The diffusivities and electron velocity are illustrated as well. The strength and direction of heat fluxes are determined through the relative strength of plasma temperature, density profiles as well as other associated scale lengths. Namely, the balance between temperature and density gradient driven flows plays an essential role in the direction of the heat flux. Moreover, electron heat pinch is observed in Fig. 4. A similar conclusion can be found in previous research [23] in which the heat pinch was determined by the ∇n component. Such a finding indicates a mechanism for heat flux pinch. Also, the results may be valuable for exploring the improvement of energy confinement. However, the heat pinch may require specified conditions, thus further underlying investigation will be needed in future work.

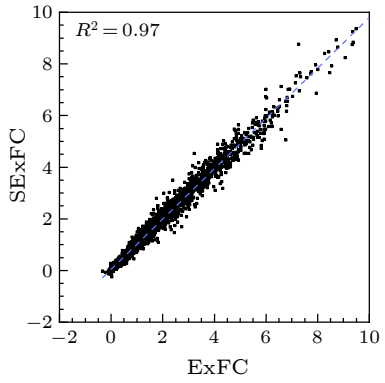

Fig. 5. Regression histograms of electron heat flux $\langle Q_e \rangle_r$ comparing between SExFC model and ExFC simulations.

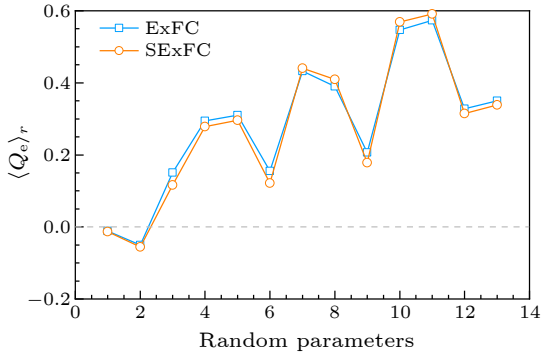

Fig. 6. $\langle Q_e \rangle_r$ as a function of random parameters selected out of databases comparing between SExFC predictions and ExFC simulations. The dashed line represents the $\langle Q_e \rangle_r \sim 0$.

On the other hand, for a credible machine learning model, further comparisons between SExFC and ExFC are required. Figure 5 shows the regression plot for each of the outputs of the NN ensemble. The regression plot is obtained by feeding the validation data set into the SExFC regression and the ExFC models. The distribution of points along the line with slope unity demonstrates that the NN-based model can predict results of the full ExFC calculation with accuracy. The training data of radial averaged electron heat flux ($\langle Q_e \rangle_r$) is considered with the coefficient of determination metric $\Re^2 = 0.97$. A further comparison of $\langle Q_e \rangle_r$ between SExFC predictions and ExFC simulations is displayed in Fig. 6. By giving random plasma parameters selected out of the databases, the prediction results of SExFC are approximative to the simulation results of ExFC. The primary characteristics of transport can be captured by the SExFC.

Finally, in this work, a framework for a machine learning-based surrogate model is established and constructed, which is for gyro-fluid electrostatic toroidal plasma simulations with a global effect. The surrogate model, SExFC, is trained to predict the type of dominant turbulence, radially averaged fluxes, and radial profiles of perturbations in the nonlinear phase, including the electron temperature $T_e(r)$, ion temperature $T_i(r)$ and density $n(r)$, as well as the corresponding electron heat flux $Q_e(r)$, ion heat flux $Q_i(r)$ and particle flux $\Gamma(r)$. Furthermore, the SExFC may also capture features of special inward transport. With the ability for real-time prediction, the possibility of taking physics-based turbulent transport information from massively parallel simulations into plasma control may come true.

Acknowledgment. This work was supported by the National Natural Science Foundation of China (Grant Nos. 12205035, 11925501, 12275071, and U1967206).

References

[1] Humphreys D, Kupresanin A, Boyer M D, Canik J, Chang C S, Cyr E C, Granetz R, Hittinger J, Kolemen E, Lawrence E, Pascucci V, Patra A, and Schissel D 2020 *J. Fusion Energy* **39** 123
[2] Degrave J, Felici F, Buchli J, Neunert M, Tracey B, Carpanese F, Ewalds T, Hafner R, Abdolmaleki A, de Casas D L, Donner C, Fritz L, Galperti C, Huber A, Keeling J, Tsimpoukelli M, Kay J, Merle A, Moret J M, Noury S, Pesamosca F, Pfau D, Sauter O, Sommariva C, Coda S, Duval B, Fasoli A, Kohli P, Kavukcuoglu K, Hassabis D, and Riedmiller M 2022 *Nature* **602** 414
[3] Kates-Harbck J, Svyatkovskiy A, and Tang W 2019 *Nature* **568** 526
[4] Joung S, Kim J, Kwak S, Bak J G, Lee S G, Han H S, Kim H S, Lee G, Kwon D, and Ghim Y C 2020 *Nucl. Fusion* **60** 016034
[5] Abbate J, Conlin R, and Kolemen E 2021 *Nucl. Fusion* **61** 046027
[6] Zheng W, Wu Q Q, Zhang M, Chen Z Y, Shang Y X, Fan J N, Pan Y, and Team J T 2020 *Plasma Phys. Control. Fusion* **62** 045012
[7] Böckenhoff D, Blatzheim M, Hölbe H, Niemann H, Pisano F, Labahn R, Pedersen T S, and The W7-X Team 2018 *Nucl. Fusion* **58** 056009
[8] Schmidhuber J 2015 *Neural Netw.* **61** 85
[9] Rea C, Montes K J, Erickson K G, Granetz R S, and Tinguely R A 2019 *Nucl. Fusion* **59** 096016
[10] Citrin J, Breton S, Felici F, Imbeaux F, Aniel T, Artaud J F, Baiocchi B, Bourdelle C, Camenen Y, and Garcia J 2015 *Nucl. Fusion* **55** 092001
[11] Meneghini O, Smith S P, Snyder P B, Staebler G M, Candy J, Belli E, Lao L, Kostuk M, Luce T, Luda T, Park J M, and Poli F 2017 *Nucl. Fusion* **57** 086034
[12] Poli F M 2018 *Phys. Plasmas* **25** 055602
[13] Doyle E J, Houlberg W A, Kamada Y, Mukhovatov V, Osborne T H, Polevoi A, Bateman G, Connor J W, Cordey J G, Fujita T, Garbet X, Hahm T S, Horton L D, Hubbard A E, Imbeaux F, Jenko F, Kinsey J E, Kishimoto Y, Li J,

Luce T C, Martin Y, Ossipenko M, Parail V, Peeters A, Rhodes T L, Rice J E, Roach C M, Rozhansky V, Ryter F, Saibene G, Sartori R, Sips A C C, Snipes J A, Sugihara M, Synakowski E J, Takenaga H, Takizuka T, Thomsen K, Wade M R, Wilson H R, ITPA Transport Physics Topical Group, ITPA Confinement Database and Modelling Topical Group, and ITPA Pedestal and Edge Topical Group 2007 *Nucl. Fusion* **47** S18
[14] Horton W, Hu B, Dong J Q, and Zhu P 2003 *New J. Phys.* **5** 14
[15] Allen L and Bishop C M 1992 *Plasma Phys. Control. Fusion* **34** 1291
[16] Wakasa A, Murakami S, Itagaki M, and Oikawa S I 2007 *Jpn. J. Appl. Phys.* **46** 1157
[17] Lister J B and Schnurrenberger H 1991 *Nucl. Fusion* **31** 1291
[18] Clayton D J, Tritz K, Stutman D, Bell R E, Diallo A, LeBlanc B P, and Podestà M 2013 *Plasma Phys. Control. Fusion* **55** 095015
[19] Svensson J, von Hellermann M, and König R W T 1999 *Plasma Phys. Control. Fusion* **41** 315
[20] Vega J, Murari A, Dormido-Canto S, Moreno R, Pereira A, Acero A, and Contributors J E 2014 *Nucl. Fusion* **54** 123001
[21] Dong G, Wei X, Bao J, Brochard G, Lin Z, and Tang W 2021 *Nucl. Fusion* **61** 126061
[22] Liu Y Q, Lao L, Li L, and Turnbull A D 2020 *Plasma Phys. Control. Fusion* **62** 045001
[23] Nordman H, Strand P, and Weiland J 2001 *Plasma Phys. Control. Fusion* **43** 1765
[24] Li H, Li J Q, Fu Y L, Wang Z X, and Jiang M 2022 *Nucl. Fusion* **62** 036014
[25] Beer M A 1995 *Ph.D. Thesis* (Princeton University)
[26] Garbet X, Garzotti L, Mantica P, Nordman H, Valovic M, Weisen H, and Angioni C 2003 *Phys. Rev. Lett.* **91** 035001
[27] Garbet X, Dubuit N, Asp E, Sarazin Y, Bourdelle C, Ghendrih P, and Hoang G T 2005 *Phys. Plasmas* **12** 082511
[28] Nordman H, Weiland J, and Jarmén A 1990 *Nucl. Fusion* **30** 983
[29] Li H, Fu Y L, Li J Q, and Wang Z X 2021 *Plasma Sci. Technol.* **23** 115102
[30] Ryter F, Angioni C, Peeters A G, Leuterer F, Fahrbach H U, and Suttrop P 2005 *Phys. Rev. Lett.* **95** 085001
[31] Hoang G T, Bourdelle C, Garbet X, Giruzzi G, Aniel T, Ottaviani M, Horton W, Zhu P, and Budny R V 2001 *Phys. Rev. Lett.* **87** 125001
[32] Baker D R *et al.* 2000 *Nucl. Fusion* **40** 1003
[33] Garzotti L, Valovič M, Garbet X, Mantica P, and Parail V (JET EFDA Contributors) 2006 *Nucl. Fusion* **46** 994
[34] Fröjdh M, Strand P, Weiland J, and Christiansen J 1996 *Plasma Phys. Control. Fusion* **38** 325